ELSEVIER

Journal of Power Sources 61 (1996) 193–200

JOURNAL OF POWER SOURCES

Carbon monoxide poisoning of platinum–graphite catalysts for polymer electrolyte fuel cells: comparison between platinum-supported on graphite and intercalated in graphite

J.Y. Tilquin [1,a,*], R. Côté [a], D. Guay [a], J.P. Dodelet [a,*], G. Denès [b]

[a] *INRS–Energie et Matériaux, CP 1020, Varennes, Que., J3X 1S2 Canada*

[b] *Chemistry Department, Concordia University, Montréal, Que., H3G 1M8 Canada*

Abstract

Platinum intercalated in graphite and Pt supported on graphite have been synthesized as catalysts for polymer electrolyte fuel cells in order to test the effect of carbon monoxide adsorption on their electrochemical properties. These materials have been characterized by X-ray diffraction, scanning electron microscopy, neutron activation analysis and cyclic voltammetry in Nafion-based films in contact with H_2SO_4 solution at pH 0.5. Pt intercalates are indeed tridimensional Pt cluster inclusions in a perturbed graphite matrix. Hydrogen electrosorption measurements demonstrate that Pt supported on graphite has three times more active sites than Pt intercalated in graphite even if Pt loadings (16 ± 4 Pt wt.%) and the size of Pt clusters (3.4 ± 0.4 nm) are similar for both catalysts. Pt supported on graphite and intercalated in graphite are equally poisoned by carbon monoxide.

Keywords: Carbon monoxide poisoning; Platinum; Polymer electrolyte fuel cells; Graphite

1. Introduction

Polymer electrolyte fuel cells (PEFCs) are potentially highly efficient electricity generators. They have also other inherent qualities such as the possibility to obtain high power density (especially since the development of the Dow membrane); they are pollution free, function at low temperature, have a fast response and high robustness. PEFCs are therefore an attractive alternative to the internal combustion engine in all areas of ground transportation [1–7].

The fuel of choice for the electric vehicle needs to be readily available. In the long term, on-board use of hydrogen is contemplated but it still requires important advances in hydrogen storage technology. In the mean time practical fuels are, for instance, kerosene or methanol. The latter one has a definite advantage: it is easily reformed in the temperature range of 250 to 300 °C. All other hydrocarbon fuels, including ethanol, require the use of higher temperatures to liberate hydrogen [7].

Reforming technologies (steam-, partial oxidation-, autothermal reforming) are well established. However, when a reformate is used, poisoning of the anode catalyst becomes an important consideration. The poisoning of platinum by carbon monoxide is reported to arise from the dual site replacement of one H_2 molecule by two CO molecules on the Pt surface [8,9]. Tests in PEFCs indicate that more than about 10 ppm of CO in the gas stream begin to impact cell performances [10,11]. The CO concentration at the exhaust of the reformer is governed by the equilibrium of the water shift reaction ($CO + H_2O \rightleftarrows CO_2 + H_2$) at the running temperature of the reformer. The H_2-rich fuel gas mixture typically contains 70–80% H_2, 20–30% CO_2 and 0.1–1.0% CO [12]. CO is then removed from the reformate gas stream by selective oxidation.

It is certain that a more poison-tolerant catalyst would ease the purity concern of the reformate. Several attempts were undertaken in that direction.

Gottesfeld and Pafford [13] have demonstrated an approach to remedy to CO poisoning by bleeding a few percent of O_2 into the H_2 line. It has the effect of oxidizing adsorbed CO to CO_2, which is harmless by itself for the catalyst. However, this approach results also in fuel loss by direct reaction with O_2.

Bifunctional metallic electrocatalysts of the type Pt–Ru or Pt–Sn were also found to be more tolerant to CO poisoning. These catalysts have mainly been studied in phosphoric acid

* Corresponding authors.

[1] Permanent address: Université Catholique de Louvain, Laboratoire de Chimie Inorganique et Analytique, place Louis Pasteur 1, 1348 Louvain-la-Neuve, Belgique.

PII S0378-7753(96)02354-3

fuel cells (PAFCs) but experiments with Pt–Ru in PEFCs indicate that, at the low operating temperature prevailing in PEFCs, the deleterious effect of CO on Pt–Ru catalysts are not significantly different from that observed with a Pt catalyst [14]. The search for an efficient anode catalyst showing improved tolerance to CO poisoning at low temperature is thus still going on.

In the present study, we propose a physical approach to the problem. It is based on the use of a Pt–graphite intercalation compound to hinder the diffusion of CO molecules to Pt while H_2 would still have free access to the metal. Such a preferential diffusion of H_2 versus CO was indeed already observed by Sirokman et al. [15] in a Ni–graphite intercalation compound. Pt–graphite intercalation compounds were therefore synthesized, characterized and tested electrochemically in half-cell conditions close to those used in PEFCs. The importance of CO poisoning for catalysts made of Pt incorporated in graphite was compared with that of Pt supported on graphite.

2. Experimental

2.1. Material preparation

Graphite (KS6 from Lonza, Switzerland) with an average particle size of 6 μm was used in all preparations. A fine graphite powder was chosen because most electrocatalytic applications require small particles to host the catalyst. All chemicals used in material preparation were at least ACS grade. Argon was of high purity.

2.1.1. Preparation of Pt-supported-on-graphite catalysts

Pt-supported-on-graphite catalysts were prepared by the method described by Zeng and Hampden–Smith [16]. $PtCl_2$ (0.36 g) and KS6 graphite (1.01 g) were suspended in 30 ml of anhydrous pyridine. The suspension was refluxed under Ar for 2 h to obtain a uniform dispersion of $PtCl_2$ on the graphite particles. Toluene (50 ml) was then added to the hot pyridine suspension and 10 ml of toluene were distilled to remove any trace of water. The suspension was allowed to cool to room temperature and 5 ml of a 1 M solution of triethylborohydride in toluene was then added dropwise under stirring. After stirring for 6 h at room temperature, the suspension was heated for 1 h and allowed to cool down. The reaction product was filtered under Ar and rinsed successively with toluene, acetone, methanol and water. It was dried at 80 °C in air for 12 h and finally weighed (1.27 g).

2.1.2. Preparation of the Pt(IV) chloride–GIC precursor and Pt–GICs catalysts

Platinum–graphite intercalation compounds (Pt–GICs) were prepared by chemical reduction of a precursor, the Pt(IV) chloride–graphite intercalation compound (Pt(IV) chloride–GIC).

2.2. Preparation of the $PtCl_4$–GIC precursor

Hydrated hexachloroplatinic acid ($H_2PtCl_6 \cdot nH_2O$, 0.80 g) was introduced in a flask under Ar and covered with 20 ml of $SOCl_2$. The solution became slightly yellow but most of the H_2PtCl_6 did not dissolve in $SOCl_2$. KS6 graphite (1.18 g) was then added. The slurry was first stirred under Ar for 48 h, then it was refluxed for 1 h and cooled to room temperature. At the end of this procedure, no H_2PtCl_6 crystals remained on the inner-wall of the flask. This indicated that the intercalation reaction was completed. The solution was then diluted with 50 ml of toluene. The reaction product was filtered, washed with toluene, dried at 80 °C for 12 h and finally weighed (1.75 g). It was previously demonstrated [17] by neutron activation analysis that the Pt(IV) chloride–GIC intercalate obtained in these experimental conditions contains 3.84 chlorine atoms for each platinum even if H_2PtCl_6 is used in the preparation.

2.3. Preparation of the Pt–GICs catalysts

Pt–GICs were prepared by reduction of Pt(IV) chloride–GIC either by reaction with potassium–naphthalene in tetrahydrofurane (THF) or by reaction with free electrons (obtained from the reaction of potassium metal) in liquid ammonia.

For the first reduction method, THF was first refluxed under Ar on potassium metal for more than three days before being distilled. Naphthalene (0.17 g) was introduced under Ar in a three-necked flask and covered with 55 ml of freshly distilled THF.

The solvent was transferred with a syringe in order to avoid contact with air. A lump of potassium was then added to the naphthalene–THF solution which turned progressively deep green as the result of the formation of the aromatic anion radical. Pt(IV) chloride–GIC (0.43 g) was then added to the solution and the slurry was stirred under Ar at room temperature for 24 h. The potassium in excess was removed from the flask before filtering the reaction product. The latter was then washed successively with acetone, methanol, and water. It was dried at 80 °C for 12 h and finally weighed (0.42 g).

For the second reduction method, anhydrous ammonia was liquified by transfer from a gas cylinder to a three-necked flask purged with Ar through a condenser cooled with dry ice. Potassium metal (0.3 g) was dissolved in liquid ammonia (50 ml) maintained at −78 °C with a dry ice–methanol bath, before adding Pt(IV) chloride–GIC (0.47 g). The slurry was stirred at −78 °C for 2 h, then the cooling bath was removed and ammonia was allowed to evaporate in a stream of Ar. The potassium in excess was destroyed by the slow addition of 20 ml of methanol. The reaction product was filtered under Ar and rinsed with methanol and water. It was dried at 80 °C for 12 h and finally weighed (0.43 g).

It was previously demonstrated [17] that the inclusion of Pt in graphite is obtained by both reduction methods.

2.4. Material characterization

X-ray powder diffraction was performed on a PW1050-2S Philips X-ray powder diffractometer automated with a Sietronics SIE system. The Ni-filtered Kα radiation of Cu ($\lambda = 1.54178$ Å) was used. The powdered samples were pressed in a 21 mm × 15 mm window of a Plexiglass holder which generates a broad and low amplitude scattering peak between $2\theta = 10$ and 20°. The X-ray diffraction (XRD) patterns were collected in the $\theta/2\theta$ step-scanning mode with a step size of 0.02° (2θ).

A Jeol-JSM 6300F instrument was used for scanning electron microscope (SEM) measurements. The materials were dispersed by ultrasonic stirring in THF and deposited on Al holders. The micrographs were recorded in the secondary electron imaging mode. Many observations were necessary to get SEM micrographs representative of the entire sample.

Elemental analyses were performed by neutron activation.

Electrochemical measurements were conducted in an air-tight three-compartment electrochemical cell at room temperature. The electrolyte was H_2SO_4, pH 0.5. The working electrode was a thin layer of Nafion-impregnated catalyst cast on a vitrous carbon disk held in a Teflon cylinder. The catalyst layer was obtained the following way: (i) a slurry was first prepared by sonicating for 1 h a mixture of 0.5 ml of deionized water, 12.9 mg of Pt–graphite catalyst and 0.3 ml of a Nafion solution (from Aldrich: 5 wt.% Nafion mixed with low aliphatic alcohols and 10% H_2O); (ii) 10 μl of the slurry was pipetted and spread on the carbon disk; (iii) the electrode was then dried at 80 °C for 20 min and mounted on a stainless-steel support. This procedure yields a well-defined working electrode surface (0.196 cm^2). The counter-electrode was a Pt foil (8 cm^2). A saturated calomel electrode (SCE) was used as reference.

An EG&G Princeton Applied Research Model 273 potentiostat was used in the experiments. The current–potential curves were generated and analyzed by the M270 software. The following procedure was systematically used to test the CO adsorption on the Pt–graphite catalyst:

1. The solution was deaerated by Ar bubbling (purified, Liquid Carbonic) for 2 h prior to electrochemical measurements.
2. The electrode was activated by cycling the potential between −0.21 and +1.2 V versus SCE at 50 mV s^{-1} [18]. These lower and upper potential limits were chosen near H_2 and O_2 evolution potentials, respectively. In the present study, more than 20 activation scans were necessary to obtain reproducible voltammograms displaying features in the hydrogen electrosorption region.
3. The potential was cycled between +0.25 and −0.21 V at 15 mV s^{-1} to obtain the hydrogen voltammetric profiles in Ar-saturated electrolyte. Four cycles were performed but only the last two voltammograms were recorded.
4. Carbon monoxide (high purity CO, Liquid Carbonic) adsorption was carried out at free potential by bubbling the gas for 10 min into the solution. Excess CO was removed by bubbling Ar for 30 min.
5. The potential was again cycled four times between +0.25 and −0.21 V at 15 mV s^{-1} to determine the extent of hydrogen adsorption sites poisoned by CO. As reported previously [19], this excursion through the hydrogen region does not affect the voltammetric behavior of adsorbed CO.
6. Adsorbed CO was oxidized by scanning the potential from +0.25 to −0.21 V, then to +1.2 V and back to +0.25 V. The scans were carried out twice in order to check if all adsorbed CO was oxidized during the first scan.
7. The electrode recovery was determined by following the procedure described in step 3.

3. Results and discussions

3.1. Characterization of the catalysts

The XRD of Pt supported on graphite is depicted in Fig. 1. The (002) line of graphite (▼) is practically equivalent in shape and intensity to the equivalent line of the pristine material. The two broad peaks attributed to Pt (■) indicate that the material contains small clusters of the metal. This is confirmed by the SEM micrograph in Fig. 2, where Pt clusters appear as a multitude of clear spots on the KS6 graphite flake. The Pt average particle size was calculated by the Sherrer formula, using the peak width-at-half-maximum of the most intense diffraction line, after correction for experimental broadening. This value is given in Table 1 with the Pt content (in wt.%).

The XRD of Pt(IV) chloride–GIC is presented in Fig. 3. The (002) line of graphite is of much lower intensity than that observed in Fig. 1 (compare the intensity of the (002) line in Figs. 1 and 3 with the intensity of the broad peak at low 2θ value common to all diffractograms). This confirms that intercalation of platinum chloride perturbs the graphite structure. Furthermore, the diffraction pattern also shows two new lines (●) directly related to the intercalation compound.

The XRDs of Pt–GICs were the same, irrespective of the method used to reduce Pt(IV) chloride–GIC. An example of Pt–GIC diffractogram is given in Fig. 4. It shows diffraction

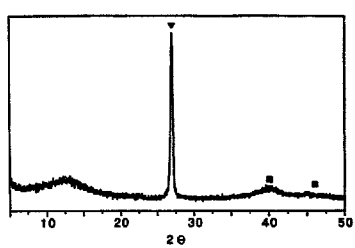

Fig. 1. XRD pattern of Pt supported on graphite (catalyst S_1).

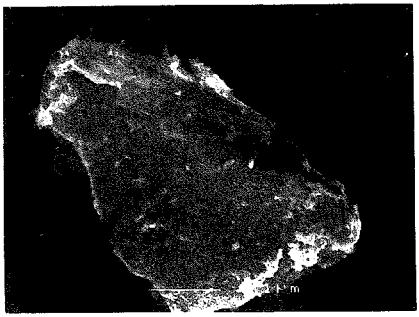

Fig. 2. SEM micrograph of Pt clusters supported on a graphite flake (catalyst S_1).

Table 1
Pt and Cl contents and mean diameter (D) of the Pt particles in both Pt-supported-on-graphite (S) and Pt–GIC (I) catalysts

Catalyst	Reduction method	Pt (wt.%) [a]	Cl (wt.%) [a]	D (nm)
I_1	K–naphthalene in THF	12.5	4.11	3.7
I_2	K in liquid NH_3	17.3	6.14	3.8
S_1	$NaBHEt_3$ in pyridine	20.0		3.1

[a] Determined by neutron activation analysis for I_1 and I_2; calculated from the starting amount of $PtCl_2$ for S_1.

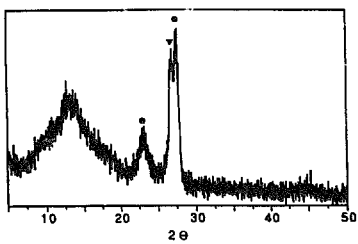

Fig. 3. XRD pattern of Pt(IV) chloride–GIC. (▼) graphite, and (●) Pt(IV) chloride–GIC.

peaks attributable to Pt (■) and KCl (●) besides the (002) line of graphite (▼). The diffraction peaks characterizing Pt(IV) chloride–GIC completely disappeared. Graphite remains strongly perturbed as evidenced by the small amplitude of its (002) line. However, the Pt and KCl diffraction lines are not broad enough to correspond to a two-dimensional spreading of these materials between the graphite planes; instead, they rather exist mainly as inclusions in graphite. This point was demonstrated elsewhere [17]. No Pt cluster or KCl crystallite is visible on the surface of the Pt–GIC flake depicted in Fig. 5. The average size of Pt inclusions is reported in Table 1 for both reduction methods used

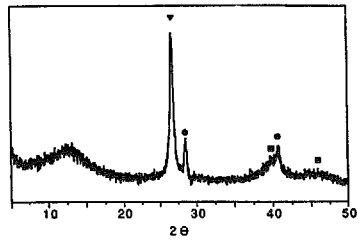

Fig. 4. XRD pattern of Pt–GIC obtained by reduction of Pt(IV) chloride–GIC by K–naphthalene in THF (catalyst I_1): (▼) graphite; (■) Pt, and (●) KCl.

Fig. 5. SEM micrograph of a flake of Pt–GIC (catalyst I_1).

in this work. Pt and Cl contents (in wt.%) of the Pt–graphite inclusion compounds are also reported in the same Table.

3.2. Electrode characterization

The Pt loadings of the electrodes and the actual area of Pt available to the oxidation of hydrogen were determined electrochemically. These results are given in Table 2, as well as the values of electrode roughness factor and those of Pt utilization.

The Pt loading of the electrodes is calculated according to Eq. (1):

Table 2
Electrode Pt loading, charges exchanged during the electro-adsorption of hydrogen atoms on Pt (Q_H), Pt surface determined electrochemically (S_{EL}), electrode roughness factor (R) and Pt utilization in both Pt supported on graphite (S) and Pt–GIC (I) catalysts

Catalyst	Pt loading (mg/cm^2)	Q_H (mC)	S_{EL} (cm^2)	R	Pt utilization (%)
I_1	0.103	0.47	2.22	11.3	28.5
I_2	0.142	0.83	3.95	20.4	37.6
S_1	0.165	2.94	14.01	71.5	95.5

$$\text{Pt loading} = \frac{M \times P_t \text{ wt.\%} \times V_1}{A \times 100 \times V_2} \quad (1)$$

where M is the catalyst mass in suspension in volume V_2; Pt wt.% is the Pt content of the catalyst (see Table 1); V_1 is the volume of the catalyst suspension spread on A, the electrode area (0.196 cm^2). The Pt loadings used in this work are in the range of values reported in Ref. [20].

The Pt surface determined electrochemically is derived from the hydrogen electro-adsorption voltammetric profiles of the electrodes. The latter curves were recorded in Ar-saturated solutions during step 3 of the procedure described in the experimental section. An example of these profiles is given in Fig. 6 for Pt supported on graphite (catalyst S_1) and Fig. 7 for Pt–GIC (catalyst I_2). As illustrated in Figs. 6 and 7, the S_1 voltammogram displays much better defined H_2 adsorption and desorption peaks than the I_2 voltammogram. The hatched area in both figures corresponds to the amount of charges, Q_H, exchanged during the electro-adsorption of hydrogen atoms on Pt. The horizontal and vertical limits of the hatched area correspond to the double-layer charging-reduction current and to the potential at the end of the second cathodic-adsorbed hydrogen peak, respectively. The Pt surface determined electrochemically, S_{EL}, is obtained according to Eq. (2):

$$S_{EL} = Q_H / Q_{H\,ref} \quad (2)$$

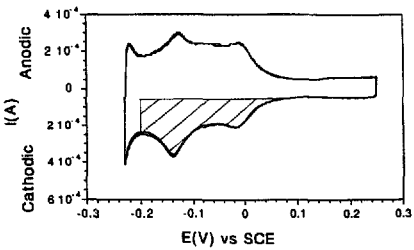

Fig. 6. Hydrogen electrosorption voltammetric profile of Pt supported on graphite (catalyst S_1) impregnated in Nafion; 15 mV s^{-1}, Ar-saturated H_2SO_4 solution at pH 0.5.

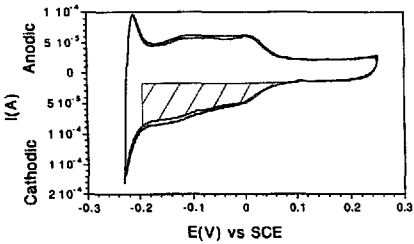

Fig. 7. Hydrogen electrosorption voltammetric profile of Pt–GIC (catalyst I_2) impregnated in Nafion; 15 mV s^{-1}, Ar-saturated H_2SO_4 solution at pH 0.5.

where $Q_{H\,ref}$ is assumed to be 0.21 mC/cm^2. It corresponds to a Pt atom surface density of 1.3×10^{15} atoms per cm^2, a value generally admitted for polycrystalline Pt electrodes [21].

The roughness factor, R, for the electrode is obtained according to Eq. (3):

$$R = \frac{S_{EL}}{A} \quad (3)$$

Roughness factors reported in Table 2 indicate that the Pt surface, measured electrochemically, is always at least one order of magnitude higher than the geometrical electrode area. It is the result of the high dispersion of Pt in the catalysts. There is, however, a large difference in R between Pt-supported-on-graphite and Pt–GICs catalysts despite their similar Pt loading.

Pt utilization in the electrode is obtained according to Eq. (4):

$$\text{Pt utilization} = N_{EL} / N_{XRD} \quad (4)$$

where N_{EL} and N_{XRD} are the number of Pt atom-gram on the surface of the electrode, determined electrochemically and from XRD measurements of the mean Pt particle size, respectively. N_{EL} is given by Eq. (5):

$$N_{EL} = Q_H / F \quad (5)$$

where F represents the Faraday constant, while N_{XRD} is given by Eq. (6):

$$N_{XRD} = \frac{\text{Pt loading} \times A \times D_i}{MW} \quad (6)$$

where MW is the mass of one atom-gram of Pt (195.08 g) and D_i represents the dispersion, i.e. the ratio between the number of Pt atoms at the surface versus the total number of Pt atoms in the crystallite. It was calculated according to the model described by Smith et al. [22], using the average Pt particle size obtained from XRD measurements. The value of D_i depends upon the structure of Pt crystallites (cubooctahedral or octahedral). Since a minimum surface energy is obtained for Pt particles that have a cubooctahedral structure [23–26] the corresponding D_i values have been used in Eq. (6). From the values presented in Table 2, it appears that about one third of the available Pt surface atoms characterizing Pt–GICs are electro-active whereas nearly all Pt surface atoms are electro-active when Pt particles are located on the graphite flakes. The absence of characteristic diffraction lines of a real intercalate for Pt–GICs and the observation of broad peaks attributable to Pt and KCl led us to conclude that Pt (and KCl) existed as tri-dimensional inclusions into the graphite host. The present results indicate that some of these inclusions should be completely surrounded by the graphite host since they are electrochemically inactive. Another possible explanation of this peculiar behavior could be the impossibility for the aqueous electrolyte to reach Pt inclusions residing deeply into the graphite perturbed structure.

3.3. CO poisoning of the catalysts

CO adsorption was performed following step 4 of the procedure described in the experimental section. Step 5 of the procedure was then performed to obtain the cyclic voltammograms displayed in Fig. 8, curve (b), for Pt supported on graphite. For comparison, curve (a) of Fig. 8 also depicts the voltammogram obtained before CO adsorption, during step 3 of the procedure.

After CO poisoning, curve (b) of Fig. 8 corresponds only to the charge of the double layer. Any hydrogen electrosorption feature disappeared indicating that CO occupies now all the H atom adsorption sites. Similar results were also obtained for both Pt–GIC catalysts. Consequently, contrary to what might be expected on the basis of H_2 and CO molecular sizes and the preferential diffusion of H_2 versus CO in Ni intercalation compounds [15], there is no particular tolerance toward CO for three-dimensional Pt inclusions in graphite.

Fig. 9 presents the succession of voltammograms recorded when the potential is scanned according to step 6 of the procedure described in the experimental section. The first scan (curve (a)) does not show electrosorption peaks for hydrogen since the entire surface of Pt in the electrode is still poisoned with CO in that potential region. A sharp oxidation peak, however, appears on the anodic scan of curve (a). Its

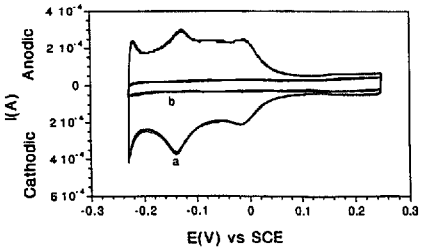

Fig. 8. Hydrogen electrosorption voltammetric profile corresponding to Pt supported on graphite (catalyst S_1) impregnated in Nafion; 15 mV s^{-1}, H_2SO_4 solution at pH 0.5; (a) Ar-saturated electrolyte, and (b) after CO adsorption.

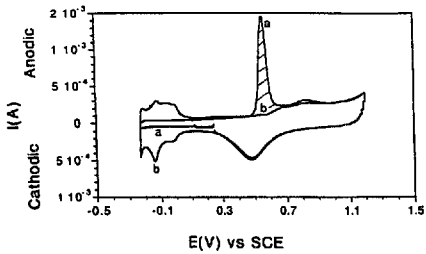

Fig. 9. Cyclic voltammograms for the electro-oxidation of CO poisoning Pt supported on graphite impregnated in Nafion; 15 mV s^{-1}, H_2SO_4 solution at pH 0.5; (a) first potential scan, and (b) second potential scan.

maximum is located at 0.559 V. This peak is related to CO oxidation. The anodic wave, associated with the formation of a monolayer of Pt oxygenated species, is observed at more anodic potential. The reduction wave located at about 0.5 V on the cathodic scan of both curves of Fig. 9 are due to the reduction of these Pt oxygenated species.

Voltammograms obtained for Pt–GICs catalysts after CO poisoning are similar to the ones presented in Fig. 9 for Pt supported on graphite. In these voltammograms, the shape and multiplicity of the CO oxidation peak are the same indicating that the CO binding sites are equivalent on all Pt electrodes already investigated [27]. However, the position of the peak maximum as well as the formation of oxygenated species shifted slightly to more anodic values for intercalated materials than for Pt supported on graphite. The position of the maximum for the CO oxidation peak are reported in Table 3.

According to the view presented by Beccdelièvre et al. [28], the oxidation of adsorbed CO requires the presence on the surface of another electrochemically formed oxygenated species. Thereby, the experimental parameters having an influence on the potential at which the formation of Pt-oxygenated species occurs will also have an influence on the position at which CO oxidation becomes possible. This is the basic idea for the use of Pt–Ru alloy catalysts in PAFCs to tolerate traces of CO in H_2 fuel. On this material, oxygenated species are generated at less anodic potential than on pure Pt, providing thereby at a lower anodic potential, the oxygen required for CO oxidation [29,30]. Therefore, trying to explain why the peak potential for CO oxidation differs for Pt supported on graphite and Pt included in graphite is equivalent to ask why the onset potential for formation of oxygenated species is different for these materials.

There is no reason to attribute this shift to a particle size effect, since the clusters of both Pt supported on graphite and Pt included in graphite are about of the same size, see Table 1.

Such a potential shift could be due to the specific adsorption of Cl^- anions on the surface of the Pt clusters in the Pt–GICs materials. This effect has already been reported elsewhere [28] for a Pt single crystal electrode exposed to Cl^- anions added to the H_2SO_4 electrolyte. Due to their specific adsorption, anions like Cl^- inhibit the formation of oxygenated species on the surface of Pt, thereby delaying the oxidation of CO [28].

Table 3
Peak potential for CO oxidation (E_{max}) charge related to CO oxidation (Q_{CO}), fractional coverage of CO linked linearly to Pt (θ_{CO}) for both Pt supported on graphite (S) and Pt–GIC (I) catalysts

Catalyst	E_{max} (V vs. SCE)	Q_{CO} (mC)	θ_{CO}
I_1	0.583	0.907	0.973
I_2	0.601	1.632	0.984
S_1	0.559	5.390	0.916

KCl is present as inclusions in both I_1 and I_2 Pt intercalated materials. However, these KCl inclusions are not able to dissolve into the electrolyte. They have therefore no role in the anodic shift of the CO electro-oxidation peak. Another explanation for that shift would be that the active Pt inclusions in the intercataled materials are more difficult to reach by the reacting molecules than Pt clusters located on the surface of the graphite flakes. If the formation of Pt-oxygenated species requires more overvoltage, so will also the electro-oxidation of CO. Since Pt utilization in intercalated material is only about one third of its possible maximum value (Table 2), it is possible that only Pt clusters, located near the entrance of the graphite galleries, are accessible to the electrolyte. This could also explain the poor definition of the H atom electrosorption voltammetric profile presented in Fig. 7.

Quantitative values of the CO surface concentration and hence of the fractional coverage θ_{CO} can be deduced from the coulombic charge corresponding to the CO oxidation peak after correction for the capacitive contribution. Weaver et al. [31] demonstrated that in sulfuric acid electrolytes, the non-faradic contribution is equal to the corresponding charge obtained in absence of CO, i.e. in the electrolyte alone, the background current being small and featureless in the potential range where CO electro-oxidation occurs. Therefore, the coulombic charge related to CO oxidation, Q_{CO}, corresponds to the area comprised between the first and second scan of the voltammogram recorded according to step 6 of the experimental procedure (hatched area in Fig. 9).

If each CO is linearly linked to Pt, there is one adsorption site and two electrons exchanged per Pt site involved in the electro-oxidation of CO. The fractional coverage of CO in these conditions is given by Eq. (7):

$$\theta_{CO} = 0.5 Q_{CO} / Q_H \quad (7)$$

Q_{CO} and I_{CO} are given in Table 3 for all the catalysts studied. The reported I values indicate that the fractional coverage of the intercalates by linearly linked CO is close to unity, which is in agreement with their voltammetry. As far as Pt supported on graphite is concerned, θ_{CO} value being less than unity can be explained by assuming that part of CO is adsorbed on more than one Pt site.

4. Conclusions

Platinum–graphite intercalation compounds were contemplated as a possibility to solve CO poisoning problems of catalysts used as anode in PEFCs, on the basis of a preferential diffusion of H_2 versus CO into the catalyst. The Pt–GICs that were synthesized are poisoned by CO like Pt supported on graphite which was used as a comparison in this study. However, characterization of Pt–GICs demonstrated that they are not real intercalates, where the metal should be spread bi-dimensionally; rather, they contain three-dimensional Pt inclusions embedded in a perturbed graphite structure. Furthermore, the Pt utilization measured by electrosorption of hydrogen demonstrated that there is a large difference between the number of electro-active sites for Pt supported on graphite and Pt intercalated in graphite even if Pt loadings and the size of Pt clusters are similar for both catalysts. It is possible that some Pt inclusions are completely surrounded by the host matrix and/or that some Pt inclusions reside too deeply in the graphite to be reachable for proton exchange with the electrolyte. Experiments are underway to obtain real two-dimensional Pt intercalates using electrochemical synthesis that were already successful for Co, Fe and Cu graphite intercalates [32–34].

Acknowledgements

We would like to thank G. Veilleux for his help with SEM measurements and CANMET LRDE for the use of their electron microscope. One author (JYT) is endebted to NATO for financial support.

References

[1] K.B. Prater, *J. Power Sources, 37* (1992) 181.
[2] R. Lemons, J. Eberhardt, A. Landgrebe, D. MacAuther, R. Savenell, S. Swathirajan, D. Wilson and M. Wilson, *Crit. Rev. Surf. Chem., 2* (1993) 297.
[3] M.Y.C. Woo, *Precious Met., 17* (1993) 475.
[4] P. Patil and P. Zegers, *J. Power Sources, 49* (1994) 169.
[5] A. Appleby, *Int. J. Hydrogen Energy, 19* (1994) 175.
[6] R.H. Williams, *Technol. Rev.*, (Apr.) (1994) 21.
[7] J.P. Schoesmith, R.D. Collins, M.J. Oakley and D.K. Stevenson, *J. Power Sources, 49* (1994) 129.
[8] W. Vogel, J. Lundquist, P. Ross and P. Stonehard, *Electrochim. Acta, 20* (1975) 79.
[9] P. Ross and P. Stonehard, *Electrochim. Acta, 21* (1976) 441.
[10] S. Gottesfeld, Polymer Electrolyte Fuel Cells: Potential Transportation and Stationary Applications, No. 10, *EPRI/GRI Fuel Cell Workshop on Technology Research and Development*, Stonehart Associates, Madison, Connecticut, 1993.
[11] J.C. Amphlett, R.M. Baumert, R.F. Mann, B.A. Peppely, P.R. Roberge and A. Rodrigues, *Prep. Pap. Am. Chem. Soc., Div. Fuel Chem., 38* (1993) 1477.
[12] K. Prater, *J. Power Sources, 29* (1990) 239.
[13] S. Gottesfeld and J. Pafford, *J. Electrochem. Soc., 175* (1988) 2651.
[14] M.S. Wilson, Ch.R. Derouin, J.A. Valerio and S. Gottesfeld, *Proc. Intersociety Energy Conversion Engineering Conf.*, Vol. 28, 1993, p. 1203.
[15] G. Sirokman, A. Mastalir, A. Molnar, M. Bartok, Z. Schay and L. Guczi, *Carbon, 28* (1990) 35.
[16] D. Zeng and M.J. Hampden-Smith, *Chem. Mater., 5* (1993) 681.
[17] J.-Y. Tilquin, R. Côté, G. Veilleux, D. Guay, G. Denès and J.P. Dodelet, *Carbon, 33* (1995) 1265.
[18] M. Hayes and A.T. Kuhn, *Appl. Surf. Sci., 6* (1980) 1.
[19] J.M. Léger, B. Beden, C. Lamy and S. Bilmes, *J. Electroanal. Chem., 170* (1984) 305.
[20] S. Srinivasan, in O.J. Murphy, S. Srinivasan and B.E. Conway (eds.), *Electrochemistry in Transition*, Plenum, New York, 1992, p. 577.
[21] R. Woods, *Electroanal. Chem., 9* (1976) 1.
[22] G.V. Smith, A. Malnar, M.M. Khan, D. Ostgard and N. Yoshida, *J. Catal., 98* (1986) 502.
[23] S.W. Wang, L.M. Falicov and A.W. Searcy, *Surf. Sci., 143* (1984) 609.

[24] M.L. Sattler and P.N. Ross, *Ultramicroscopy, 20* (1986) 21.
[25] K. Kinoshita, *J. Electrochem. Soc., 137* (1990) 845.
[26] F.M. Mulder, T.A. Stegink, R.C. Thiel, L.J. de Jongh and G. Schmidt, *Nature, 367* (1994) 716.
[27] B. Beden, C. Lamy, N.R. de Tacconi and A.J. Arvia, *Electrochim. Acta, 35* (1990) 691.
[28] A.M. de Becdelièvre, J. de Becdelièvre and J. Clavilier, *J. Electroanal. Chem., 294* (1990) 97.
[29] H.A. Gasteiger, N. Markovic, P.N. Ross and E.J. Cairns, *J. Phys. Chem., 98* (1994) 617.
[30] R. Ianniello, V.M. Schmidt, U. Stimming, J. Stumper and A. Wallace, *Electrochim. Acta, 39* (1994) 1863.
[31] M.J. Weaver, S.C. Chang, L.W.H. Leung, X. Jiang, M. Rubel, M. Szklarczyk, D. Zurawski and A. Wieckowski, *J. Electroanal. Chem., 327* (1992) 247.
[32] G.K. Nguessan and P. Touzain, *Synth. Met., 34* (1989) 267.
[33] M. Crespin, K. Tatsumi, H. Sakakihara, H. Shioyama and F. Beguin, *Mol. Cryst. Liq. Cryst., 244* (1994) 215.
[34] P. Scharff and R. Optiz, *Mol. Cryst. Liq. Cryst., 244* (1994) 197.